

Synthesis and study on optical properties of CeO₂-Mg(OH)₂ and inverted Mg(OH)₂-CeO₂ nanocomposites

G. Murugadoss^{a,*}, M. Rajesh Kumar^b, R. Jothi Ramalingam^c, Hamad Al-Lohedan^c, A. Ramesh Babu^d, A. Kathalingam^e, Ahmed M. Tawfeek^c

^aCentre for Nanoscience and Nanotechnology, Sathyabama Institute of Science and Technology, Chennai 600119, Tamil Nadu, India

^bInstitute of Natural Science and Mathematics, Ural Federal University, Yekaterinburg 620002, Russia

^cChemistry Department, College of Science, King Saud University, P.O. Box. 2455, Riyadh 11451, Kingdom of Saudi Arabia, Saudi Arabia

^dSchool of Electrical and Electronics, Department of Electrical and Electronics Engineering, Sathyabama Institute of Science and Technology, Chennai 600119, Tamil Nadu, India

^eMillimeter-wave Innovation Technology Research Center, Dongguk University-Seoul, Seoul 04620, South Korea

Well-crystalline CeO₂-Mg(OH)₂ and inverted Mg(OH)₂-CeO₂ nanocomposites were successfully synthesized by a facile ‘one-pot’ chemical precipitation method at low temperature. The crystal structure, morphology and optical properties of the CeO₂-Mg(OH)₂ and inverted Mg(OH)₂-CeO₂ nanocomposites were investigated using X-ray diffraction, TEM, FTIR, UV-vis absorption and PL spectrometer. The photoluminescence study revealed visible light emission for the nanocomposite. Interestingly, significant red shift observed for Mg(OH)₂-CeO₂ nanocomposites. The optical tuning nanocomposites can be used for the optoelectronic applications.

(Received July 3, 2021; Accepted November 4, 2021)

Keywords: Nanocomposites, TEM, X-ray techniques

1. Introduction

In the field of nanotechnology, the synthesis of controlled structures is crucial for the development of functional devices, with many in the field aiming for the convenience of bottom-up fabrication as opposed to timely and costly top-down methods. Over the years, numerous metal oxides namely TiO₂, ZnO, CeO₂, SnO₂, WO₃, NiO, Fe₂O₃ and CuO, etc., were used extensively in photovoltaics, supercapacitor, battery, optoelectronics and photocatalytic degradation [1–5].

Among the metal oxides, Cerium dioxide (CeO₂) is an important for combustion applications due to their special characteristics. CeO₂ has a cubic fluorite type structure with an Fm3m spatial group [6]. An important characteristic of CeO₂ is that it undergoes substantial changes in the stoichiometry of oxygen in response to changes in temperature, oxygen pressure, electric field and the presence of dopants, without undergoing changes in crystal structure [7], while the transport of oxygen through its structure results in the creation of intrinsic point defects [6]. CeO₂ shows unique redox properties and high oxygen storage capacity (OSC), which allows it to quickly switch oxidation state between Ce⁴⁺ and Ce³⁺ [8].

To control the surface reactivity and limit the electronic influence of surface defects [9], a common technique can enhance the properties of nanostructures is to create nanocomposites [10]. Magnesium oxide (MgO) as a versatile oxide material with assorted properties like large band gap, excellent thermodynamical stability, low dielectric constant and low refractive index finds

* Corresponding author: murugadoss_g@yahoo.com

extensive applications in catalysis, ceramics, toxic waste remediation, antibacterial materials, and as an additive in refractory, paint and superconductor products [11-13].

Previously, researchers have fabricated controlled ZnO–MgO (nanopillar) heterostructures [14], which may be useful in the study of chemical sensors, optical devices and scanning probes in addition to providing a reliable heterojunction material to study quantum confinement effects. Doping ZnO with MgO in a de-ionized water for produce a flat thin film, followed by a high temperature anneal, has been obtained to be especially useful in hybrid solar cell devices as a form of bandgap engineering [15-16].

Pure magnesium based precursors (magnesium metal, magnesium chloride, magnesium nitride, magnesium sulfate and other salts containing magnesium) plays a vital role in the production of high purity MgO and Mg(OH)₂ nanostructures. However, limited studies could be found dealing with the synthesis of magnesium hydroxide and magnesium oxide nanostructures from an impure precursor [17].

Hitherto, nanocomposites were synthesized using thermal evaporation [18], flame spray pyrolysis [19], sol–gel [20], chemical vapor deposition [21], hydrothermal [22], and surfactant methods [23]. However, these synthesis techniques are expensive and involve complex methods, it need precious analytical instruments, and the use of synthetic chemical and organic solvents which were harmful and not easily degraded in the environment. Thus, developing a simple ‘one-pot’ chemical method for preparation of CeO₂-Mg(OH)₂ and inverted Mg(OH)₂-CeO₂ nanocomposites remained a challenging topic of investigation. Accordingly, in the present work we report a facile route to synthesis of CeO₂-Mg(OH)₂ and inverted Mg(OH)₂-CeO₂ nanocomposites by chemical method.

2. Experimental Procedure

2.1. Preparation of CeO₂-Mg(OH)₂ and inverted Mg(OH)₂-CeO₂ nanocomposites

All chemical were used analytical grade with high purity. In a typical synthesis of CeO₂-Mg(OH)₂, 0.2 M of Cerium (III) nitrate hexahydrate (Ce(NO₃)₃·H₂O) was dissolved in 100 mL distilled water. Then 1g of polyvinylpyrrolidone (PVP) was added into the above solution. Next, 2 M of NaOH was directly added into the above solution under constant stirring at 80 °C. After 1 h, 0.2 M of Magnesium Chloride (MgCl₂·6H₂O) solution was added to the above colloidal solution and the resultant solution was stirred for another 1 h. Then, the sample washed with de-ionized water, ethanol and acetone to remove residuals and then it was dried in a hot air oven at 120 °C for 4 h. The obtained powder sample was subjected to the characterization. To synthesis Mg(OH)₂-CeO₂, the similar synthesis procedure was used with interchange the precursors of Ce(NO₃)₃·H₂O and MgCl₂·6H₂O.

2.2. Characterization

Crystal structure of the prepared samples were analysed using powder X-ray diffraction (XRD) spectrometer (Bruker Axs D8 diffractometer) equipped with Cu K α radiation ($\lambda = 1.541 \text{ \AA}$). Functional groups presence in the surface of the nanoparticles were evaluated using Fourier transform infrared spectroscopy (FTIR) using Bio-Rad (Hercules, CA) FTS-165 spectrometer. The microstructure information of CeO₂-Mg(OH)₂ and inverted Mg(OH)₂-CeO₂ nanocomposites was studied using transmission electron microscope (TEM, PHILIPS CM200). Optical absorption and band gap of the samples were estimated from UV diffused reflectance spectroscopy (DRS) using a JASCO V-670 double beam spectrophotometer. Photoluminescence (PL) spectra for the synthesized samples were recorded using a JOBIN YVON FLUROLOG-3–11 spectrofluorometer equipped with Xe lamp (Excitation wavelength = 325 nm).

3. Results and Discussion

Fig. 1(a) shows the X-ray diffraction patterns of CeO₂-Mg(OH)₂ and inverted Mg(OH)₂-CeO₂ nanocomposites, indicating mixed phases of CeO₂ and Mg(OH)₂. Individual phases of CeO₂

and $\text{Mg}(\text{OH})_2$ were observed without producing new compounds. Fig. 1(a) shows the sharp and narrow peaks belongs to $\text{Mg}(\text{OH})_2$ and other peaks belongs to CeO_2 . The CeO_2 diffraction peaks were observed at 2θ of 28.13, 33.05, 47.52, 56.53, and 59.14°, corresponding to the planes of (1 1 1), (2 0 0), (2 2 0), (3 1 1), and (2 2 2), respectively. The lattice plane indicates fluorite cubic structure (JCPDS card no.: 89-8436) of CeO_2 . The diffraction peaks of $\text{Mg}(\text{OH})_2$ were observed at 2θ of 38.24, 51.07, 58.91, 62.31, 68.42 and 72.27° corresponds to (1 0 1), (1 0 2), (1 1 0), (1 1 1), (1 0 3) and (0 0 2) planes, respectively. All the diffraction planes are corresponds to hexagonal structure (JCPDS card no.: 84-2164) of $\text{Mg}(\text{OH})_2$. In the cubic structure of CeO_2 , cation such as Ce^{4+} is in the closed packing cubic structure, and O^{2-} anions are fully occupied in the tetrahedral sites. Since all of the octahedral sites are vacant, the large vacancy is provided as an interstitial position. Other metal cations are readily substituted in the fluorite structure and also, inserted in the interstitial positions. In the cubic CeO_2 , a change in the lattice constant by substitution is greater than that in the interstitial solid solution. If Ce^{4+} cations were substituted by Mg^{2+} cations in the CeO_2 phase, the lattice constant of CeO_2 should be varied. Judging from the fact that no change in the lattice constant of the CeO_2 phase was observed in our system, it is assumed that Mg^{2+} cations are inserted in the interstitial position of CeO_2 crystallites. The crystallite size was found is to be 11.2 nm and 14.6 nm for $\text{CeO}_2\text{-Mg}(\text{OH})_2$ and inverted $\text{Mg}(\text{OH})_2\text{-CeO}_2$ nanocomposites, respectively using Debye Scherrer equation [24].

Fig. 1(b) shows FT-IR spectra of the $\text{CeO}_2\text{-Mg}(\text{OH})_2$ and inverted $\text{Mg}(\text{OH})_2\text{-CeO}_2$ nanocomposites. The peaks observed at 1636 cm^{-1} and 3420 cm^{-1} is due to the presence of $-\text{OH}$ stretching and bending, respectively, assigned to the H_2O adsorption on the surface samples. The absorption band at 2361 cm^{-1} is ascribed to the stretching vibrations of CO_2 due to adsorption of atmospheric carbon dioxide [25-27]. The band at 1076 cm^{-1} is attributed to the H^- ion [25]. In inverted $\text{Mg}(\text{OH})_2\text{-CeO}_2$ nanocomposites, the peak at 426 cm^{-1} indicated Mg-O bond stretching, which in turn confirmed that the obtained product have magnesium hydroxide.

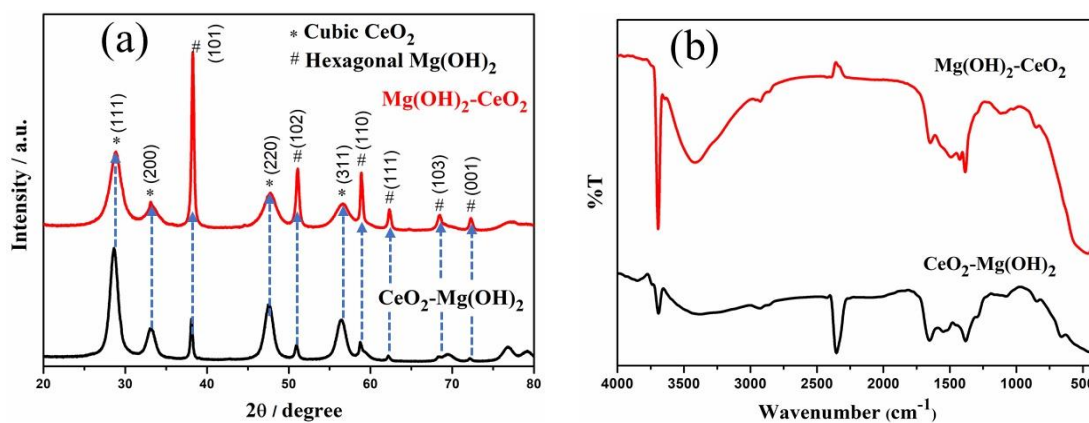


Fig. 1. (a) X-ray diffraction spectra (b) FT-IR spectra of the $\text{CeO}_2\text{-Mg}(\text{OH})_2$ and inverted $\text{Mg}(\text{OH})_2\text{-CeO}_2$ nanocomposites.

Fig. 2(a,b) shows the TEM images of different magnifications of the $\text{CeO}_2\text{-Mg}(\text{OH})_2$ nanocomposites and Fig. 3(a,b) shows TEM images of $\text{Mg}(\text{OH})_2\text{-CeO}_2$ nanocomposites. TEM images (Fig. 2(a,b) and Fig. 3(a,b)) shows that mostly agglomerated with the presence of spherical shaped grains in the nanoscale range. A mixture of grains related to both CeO_2 and $\text{Mg}(\text{OH})_2$ were observed, which gives a supporting evidence for the homogeneous mixing of both CeO_2 and $\text{Mg}(\text{OH})_2$. The average size of the particles shows about 12.3 and 15.1 nm for $\text{CeO}_2\text{-Mg}(\text{OH})_2$ and inverted $\text{Mg}(\text{OH})_2\text{-CeO}_2$ nanocomposites.

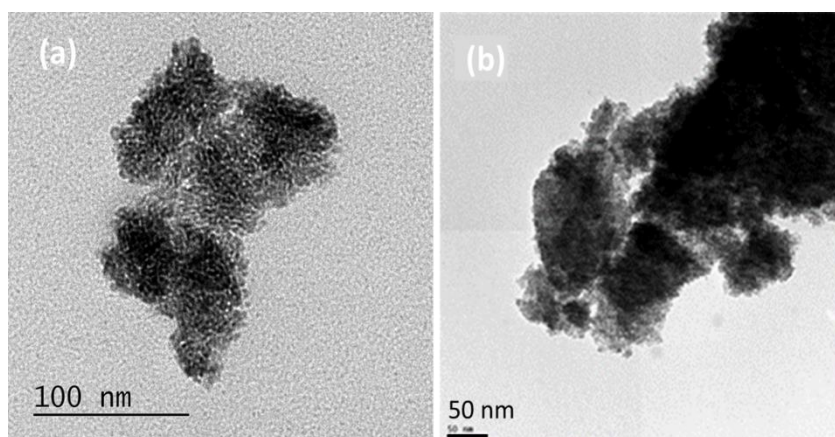


Fig. 2. (a, b) TEM images of the different magnifications of $\text{CeO}_2\text{-Mg(OH)}_2$ nanocomposites.

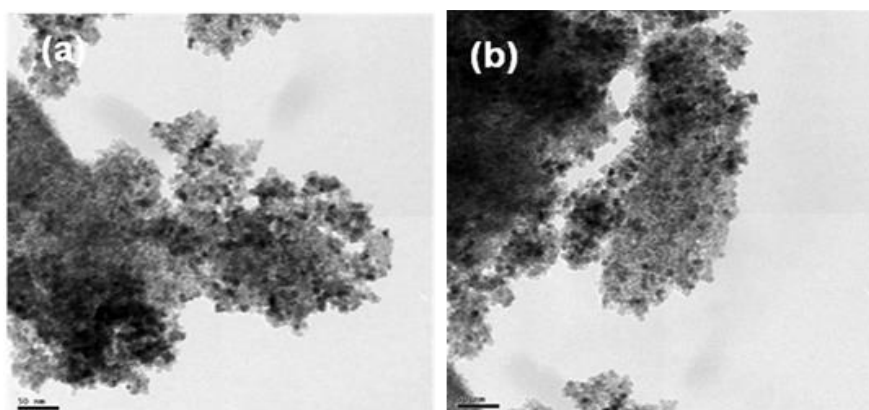


Fig. 3. (a, b) TEM images of the different magnifications of $\text{Mg(OH)}_2\text{-CeO}_2$ nanocomposites.

Fig. 4(a) shows the UV–Vis absorption spectra of $\text{CeO}_2\text{-Mg(OH)}_2$ and inverted $\text{Mg(OH)}_2\text{-CeO}_2$ nanocomposites. The nanocomposites exhibited absorption in the range between 350–400 nm corresponds to the excitation of four-fold coordinated O^{2-} anions in the edges and corners. The following formula is used to calculate the energy bandgap (E_g) using Tauc plot spectra [28]:

$$\alpha(h\nu) = A(h\nu - E_g)^{n/2} \quad (1)$$

where ' α ' and ' $h\nu$ ' represent the absorption coefficient and the light energy, ' A ' is a constant, ' E_g ' the optical bandgap and ' n ' is an integer equal to 1 for a direct bandgap and 4 for an indirect bandgap. The plot of $(\alpha h\nu)^2$ versus E_g (eV) was used for estimating the value of energy bandgap by extrapolating curve to zero absorption and shown in Fig. 4(b). The calculated value of the bandgap (E_g) was found are 3.24 and 2.81 eV for $\text{CeO}_2\text{-Mg(OH)}_2$ and inverted $\text{Mg(OH)}_2\text{-CeO}_2$ nanocomposites, respectively. The narrow band gap nanocomposite ($\text{Mg(OH)}_2\text{-CeO}_2$) can be used as an electrode material for solar cell and supercapacitor application [29,30].

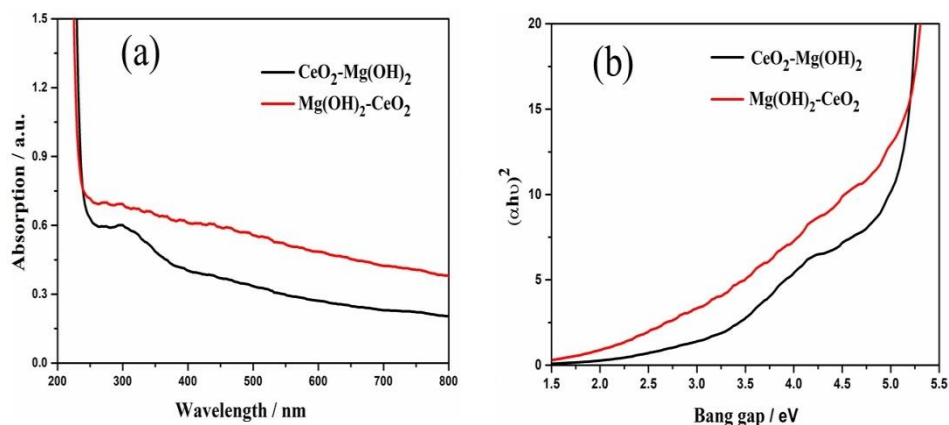


Fig. 4. (a) UV/vis spectra of the $\text{CeO}_2\text{-Mg(OH)}_2$ and inverted $\text{Mg(OH)}_2\text{-CeO}_2$ nanocomposites and (b) Tauc plots of the corresponding samples.

Fig. 5(a,b) shows the photoluminescence spectra of the $\text{CeO}_2\text{-Mg(OH)}_2$ and inverted $\text{Mg(OH)}_2\text{-CeO}_2$ nanocomposites. It shows that the broad band around 425 nm and 625 nm for $\text{CeO}_2\text{-Mg(OH)}_2$ and inverted $\text{Mg(OH)}_2\text{-CeO}_2$ nanocomposites, respectively. The PL peaks of $\text{CeO}_2\text{-Mg(OH)}_2$ and inverted $\text{Mg(OH)}_2\text{-CeO}_2$ nanocomposites are showed in blue and red wavelength region, respectively. Interestingly, the PL emission is significantly shifted towards longer wavelength side due to decreasing the band gap. The drastic changes in the PL emission by changing the compounds is indicates the role of the normal and inverted nanocomposites.

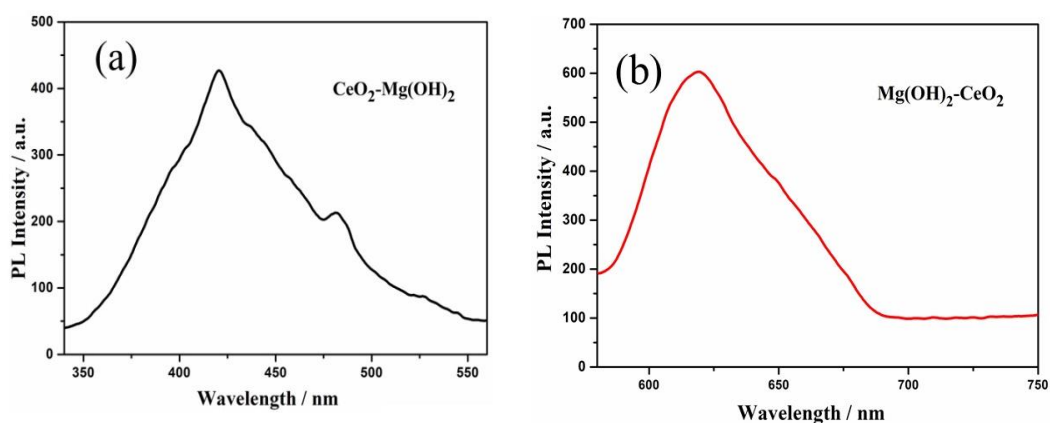


Fig. 5. (a) Photoluminescence spectra of the $\text{CeO}_2\text{-Mg(OH)}_2$ and inverted (b) $\text{Mg(OH)}_2\text{-CeO}_2$ nanocomposites.

4. Conclusion

In summary, the $\text{CeO}_2\text{-Mg(OH)}_2$ and inverted $\text{Mg(OH)}_2\text{-CeO}_2$ nanocomposite were successfully synthesized by a facile ‘one pot’ chemical method at low-temperature. A mixed crystal structure of cubic and hexagonal obtained for CeO_2 and Mg(OH)_2 , respectively. The obtained homogeneous particles from TEM showed the preparation method is adoptable for control size of the nanocomposites. Furthermore, optical study investigations implied that the ‘one-pot’ chemical method for synthesise of nanocomposites benefit to optical tune band gap by changing the precursor during the preparation.

Acknowledgments

The author R. Jothiramalingam thank for the financial support by the Researchers Supporting Project Number (RSP-2021/354), King Saud University, Riyadh, Saudi Arabia. The author Dr. G. Murugadoss thanks the Chancellor, President, and Vice Chancellor, Sathyabama Institute of Science and Technology, Chennai for the support and encouragement.

References

- [1] X. Jiang, L. Yang, P. Liu, X. Li, J. Shen, *Colloids Surf. B* **79**, 69 (2010).
- [2] G. Murugadoss, H. Kanda, S. Tanaka, H. Nishino, S. Ito, H. Imahoric, T. Umeyama, *J. Power Sources* **307**, 891 (2016).
- [3] A. M. Cruz, D. S. Martinez, E. L. Cuellar, *Solid State Sci.* **12**, 88 (2010).
- [4] J. Gu, S. Li, E. Wang, Q. Li, G. Sun, R. Xu, H. Zhang, *J. Solid State Chem.* **182**, 1265 (2009).
- [5] G. Murugadoss, D.D. Kumar, M.R. Kumar, N. Venkatesh, P. Sakthivel, *Sci. Rep.* **11**, 1080 (2021).
- [6] A. Trovarelli, World Scientific, New York (2002) 15.
- [7] J. Paier, C. Penschke, J. Sauer, *Chem. Rev.* **113**, 3949 (2013).
- [8] G. Manibalan, Y. Govindaraj, J. Yesuraj, P. Kuppusami, G. Murugadoss, R. Murugavel, M. R. Kumar, *J. Colloid and Interface Sci.* **585**, 505 (2021).
- [9] L. Schmidt-Mende, J. L. MacManus-Driscoll, *Mater. Today* **10**, 40 (2007).
- [10] S. Kim et al., *Appl. Phys. Lett.* **92**, 243108 (2008)
- [11] G. Duan, X. Yang, J. Chen, G. Huang, L. Lu, X. Wang, *Powder Technol.* **172**, 27 (2007).
- [12] M. A. Shah, A. Qurashi, *J. Alloys Compd.* **482**, 548 (2009).
- [13] W. Wang, X. Qiao, J. Chen, F. Tan, H. Li, *Mater. Charact.* **60**, 858 (2009).
- [14] Y.W. Heo, et al., *Mater. Sci. Eng. R* **47**, 1 (2004)
- [15] O.-A. Boateng, S. K. A. Kumara, M. Okuya, K. Murakami, A. Konno, K. Tennakone, Japan. *J. Appl. Phys.* **44**, 731 (2005)
- [16] D. C. Olson, S. E. Shaheen, M. S. White, W. J. Mitchell, M. F. A. M. van Hest, R. T. Collins, D. S. Ginley, *Adv. Funct. Mater.* **17**, 264 (2007)
- [17] S. Yousefi, B. Ghasemi, M. Tajally, A. Asghari, *J. Alloys and Compounds* **711**, 521 (2017).
- [18] Q. Yang, J. Sha, L. Wang, J. Wang, D. Yang, *Mater. Sci. Eng. C* **26**, 1097 (2006).
- [19] X. Yi, W. Wenzhong, Q. Yitai, Y. Li, C. Zhiwen, *Surf. Coat. Technol.* **82**, 291 (1996).
- [20] T. X. Phuoc, B. H. Howard, D. V. Martello, Y. Soong, M. K. Chyu, *Opt. Lasers Eng.* **46**, 829 (2008).
- [21] Y. Hao, G. Meng, C. Ye, X. Zhang, L. Zhang, *J. Phys. Chem. B* **109**, 11204 (2005).
- [22] G. Manibalan, G. Murugadoss, R. Thangamuthu, P. Ragupathy, R. M. Kumar, R. Jayavel, *Appl. Surf. Sci.* **456**, 104 (2018)
- [23] P. Ouraipryvan, T. Sreethawong, S. Chavadej, *Mater. Lett.* **63**, 1862 (2009).
- [24] G. Manibalan, G. Murugadoss, R. Thangamuthu, P. Ragupathy, M. R. Kumar, R. M. Kumar, R. Jayavel, *Inorg. Chem.* **58**, 13843 (2019).
- [25] N. C. S. Selvam, R. T. Kumar, L. J. Kennedy, J. J. Vijaya, *J. Alloys Compd.* **509**, 9809 (2011).
- [26] J. Zhou, S. Yang, J. Yu, *Colloids Surf. A* **379**, 102 (2011).
- [27] H. Niu, Q. Yang, K. Tang, Y. Xie, *J. Nanopart. Res.* **8**, 881 (2006).
- [28] G. Manibalan, G. Murugadoss, R. Thangamuthu, R.M. Kumar, M.R. Kumar, R. Jayavel, *J. Mater. Sci.: Mater. Electronics* **29**, 13692 (2018).
- [29] S. Krobthong, S. Nilphai, S. Choopun, S. Wongrerkrdee, *Dig. J. Nanomater. Biostructures*, **15**, 885 (2021).
- [30] R. J. Ramalingama, H. Al-Lohedan, A. M. Tawfik, G. Periyasamy, M. R. Muthumareeswaran, *Chalcogenide Letters* Vol. **17**, No. 8, August 2020, P. 423 – 428.